BAMS Article

Improving High-Impact Numerical Weather Prediction with Lidar and Drone Observations

Daniel Leuenberger, Alexander Haefele, Nadja Omanovic, Martin Fengler, Giovanni Martucci, Bertrand Calpini, Oliver Fuhrer, and Andrea Rossa

ABSTRACT: The current atmospheric observing systems fail to provide a satisfactory amount of spatially and temporally resolved observations of temperature and humidity in the planetary boundary layer (PBL) despite their potential positive impact on numerical weather prediction (NWP). This is particularly critical for humidity, which exhibits a very high variability in space and time or for the vertical distribution of temperature, determining the atmosphere's stability. Novel ground-based lidar remote sensing technologies and in situ measurements from unmanned aerial vehicles can fill this observational gap, but operational maturity was so far lacking. Only recently, commercial lidar systems for temperature and humidity profiling in the lower troposphere and automated observations on board of drones have become available. Raman lidar can provide profiles of temperature and humidity with high temporal and vertical resolution in the troposphere. Drones can provide high-quality in situ observations of various meteorological variables with high temporal and vertical resolution, but flights are complicated in high-wind situations, icing conditions, and can be restricted by aviation activity. Both observation systems have shown to considerably improve analyses and forecasts of high-impact weather, such as thunderstorms and fog in an operational, convective-scale NWP framework. The results of this study demonstrate the necessity for and the value of additional, high-frequency PBL observations for NWP and how lidar and drone observations can fill the gap in the current operational observing system.

https://doi.org/10.1175/BAMS-D-19-0119.1
Corresponding author: Daniel Leuenberger, daniel.leuenberger@meteoswiss.ch
In final form 21 February 2020

AFFILIATIONS: Leuenberger and Rossa—Federal Office of Meteorology and Climatology MeteoSwiss, Zurich, Switzerland; **Haefele, Martucci, Calpini**—Federal Office of Meteorology and Climatology MeteoSwiss, Payerne, Switzerland; **Omanovic and Fengler**—Meteomatics AG, St. Gallen, Switzerland; **Fuhrer**—Federal Office of Meteorology and Climatology MeteoSwiss, Zurich, Switzerland, and Vulcan Inc., Seattle, Washington

High-impact weather is often determined by physical processes taking place in the planetary boundary layer (PBL). The PBL temperature and moisture distributions determine to a large degree the preconvective environment and the occurrence of thunderstorms (e.g., Koch et al. 2018). Findings from impact studies and field experiments corroborate this (e.g., Crook 1996; Weckwerth et al. 2004; Browning et al. 2007; Wulfmeyer et al. 2011).

Fog and low stratus are common weather phenomena in central Europe during fall and winter and have a high socioeconomic impact (e.g., Gultepe et al. 2009; Ashley et al. 2015; Köhler et al. 2017). An accurate thermodynamic structure of the PBL in the initial conditions is crucial for successful fog forecasts using numerical weather prediction (NWP) models (e.g., Rémy and Bergot 2009). Specifically, capturing the temperature inversion at the right height and with the correct strength as well as an adequate distribution of water vapor in space and time are essential for an accurate representation of fog.

The upper-air atmospheric observing system is composed of a multitude of techniques each one with strengths and weaknesses in terms of vertical and temporal sampling, vertical range, and horizontal resolution in the PBL. Spaceborne sensors generally have very good horizontal and temporal coverage but are unable to observe in the lowest few kilometers of the atmosphere due to surface effects or clouds (Tatem et al. 2008; Balsamo et al. 2018). Radiosondes provide very high-quality and high-vertical-resolution profiles of temperature, humidity, and wind, but are generally launched only twice per day. Commercial aircraft deliver temperature and wind profiles through the Aircraft Meteorological Data Relay (AMDAR) (e.g., Petersen 2016) or Mode-S programs (KNMI 2019). Data quality matches the requirements for NWP and the spatiotemporal coverage is good around airports. However, humidity is generally not provided by those programs with a few exceptions as, for instance, a U.S. network of aircrafts equipped with a Tropospheric Airborne Meteorological Data Reporting (TAMDAR) sensor (Zhang et al. 2015, and references therein). Wind profilers provide wind information and are one of the best established PBL profiler systems. In Europe, for example, wind profilers are integrated into a network that is coordinated by the European National Meteorological Services (EUMETNET) E-PROFILE program (EUMETNET 2020).

The World Meteorological Organization (WMO) guidance for NWP applications states, that wind, temperature, and humidity profiles, particularly for the PBL, are "critical atmospheric variables, that are not adequately measured by current or planned systems," both for global and high-resolution, regional models (WMO 2018a,b). WMO's Observing Systems Capability Analysis and Review (OSCAR) tool contains a catalog of requirements for observations for various application areas (WMO 2017). These OSCAR requirements are established by internationally recognized experts and the requirements to which we refer in this study are all firm, meaning "result of actual impact studies of actual data used in actual applications of numerical or conceptual models." We therefore consider OSCAR a good reference for requirements. Table 1 shows an extract of the OSCAR requirements for global and high-resolution NWP for lower-tropospheric temperature, humidity, and wind. Three requirement levels are defined: threshold (minimum requirement for usefulness of observations), breakthrough (significant improvement of application, optimum from a cost–benefit point of view), and goal (ideal requirement, no further improvements necessary). While the above-mentioned observation systems generally meet the breakthrough requirements for quality and vertical

Table 1. List of WMO OSCAR requirements for the lower troposphere and global/high-resolution NWP application areas. Each parameter has three requirement levels: goal (G), breakthrough (B), and threshold (T) (see text for an explanation).

Variable	Application area	Level	Uncertainty	Horizontal resolution	Vertical resolution	Observation cycle	Timeliness
Temperature	Global NWP	G	0.5 K	15 km	0.3 km	60 min	6 min
		B	1 K	100 km	1 km	6 h	30 min
		T	3 K	500 km	3 km	24 h	6 h
Humidity	Global NWP	G	2%	15 km	0.3 km	60 min	6 min
		B	5%	50 km	1 km	6 h	30 min
		T	10%	250 km	3 km	12 h	6 h
Wind	Global NWP	G	1 m s^{-1}	15 km	0.5 km	60 min	6 min
		B	3 m s^{-1}	100 km	1 km	6 h	30 min
		T	5 m s^{-1}	500 km	3 km	12 h	6 h
Temperature	High resolution NWP	G	0.5 K	0.5 km	0.1 km	15 min	15 min
		B	1 K	2 km	0.25 km	60 min	30 min
		T	3 K	10 km	1 km	6 h	2 h
Humidity	High resolution NWP	G	2%	0.5 km	0.1 km	15 min	15 min
		B	5%	5 km	0.2 km	60 min	30 min
		T	10%	20 km	1 km	6 h	2 h
Wind	High resolution NWP	G	1 m s^{-1}	0.5 km	0.1 km	15 min	15 min
		B	2 m s^{-1}	2 km	0.2 km	60 min	30 min
		T	5 m s^{-1}	10 km	0.4 km	12 h	2 h

resolution, they are not able to meet the requirements for horizontal and temporal resolution for lower-tropospheric temperature and humidity. The need for additional PBL observations is also reflected in recent publications (e.g., Dabberdt et al. 2005; National Research Council 2010; Hardesty and Hoff 2012; Everett 2018).

Consequently, there is a significant gap in today's operational observing system in terms of thermodynamical quantities and wind in the PBL inhibiting detailed and reliable forecasts of high-impact weather.

There are a number of emerging technologies, which can potentially and partly fill this gap (Illingworth et al. 2019): Ground-based profilers, such as ceilometers, wind lidars, and microwave radiometers have improved in the last years and data are becoming available in international networks. While ceilometers provide information about clouds and aerosols, wind lidars about wind, only microwave radiometers (MWRs) are able to give information about temperature and humidity. Despite the limited vertical resolution of humidity and temperature profiles from MWRs, positive impact on NWP could already be demonstrated based on case studies (Caumont et al. 2016).

The aim of this paper is twofold: First, we present two novel candidate observing systems to contribute to filling the gap in the observation of the boundary layer: Raman lidar and rotary-wing unmanned aerial vehicles (UAVs), also referred to as drones. Second, we present two case studies to demonstrate, how these novel measurements can improve convective-scale NWP forecasts of high-impact weather, such as thunderstorms and fog. Finally, a short discussion on the potential of the new observing systems in a global perspective is provided.

The numerical weather prediction system

The statistical model-observation comparisons and the impact studies described in this study have been performed with the operational NWP system of the Federal Office of Meteorology

and Climatology MeteoSwiss, based on the nonhydrostatic COSMO model (Baldauf et al. 2011). The NWP system consists of a Kilometric Ensemble Data Assimilation (KENDA) system with a mesh-size of 2.2 km and 40 ensemble members, similar to that described in Schraff et al. (2016) and 20 ensemble forecasts initialized therefrom. The ensemble assimilation update step is based on the local ensemble transform Kalman filter (LETKF; Hunt et al. 2007). The lateral boundary conditions are taken from the European Centre for Medium-Range Weather Forecasts (ECMWF) deterministic and Ensemble Prediction System (EPS) forecasts and the EPS model uncertainty is accounted for with a stochastic perturbation of physical tendencies (SPPT) method. Observations from standard TEMP, SYNOP, AIREP, and wind profiler devices are included in the KENDA system. Radar surface precipitation estimates from the Swiss Radar Network are additionally assimilated with a latent heat nudging method (Stephan et al. 2008).

Raman lidar

Working principle and applications. A lidar (light detection and ranging) is an active remote sensing device, which emits a light pulse and detects the back scattered light as a function of range. Raman lidars exploit inelastic Raman scattering where the back scattered light is shifted in wavelength. For vibrational–rotational Raman scattering, this wavelength shift is characteristic of a given molecule, for instance water vapor, and hence allows to measure its concentration (Cooney 1972b). For pure rotational scattering, the intensity of the back scattered light (mainly by N_2 and O_2 molecules) depends strongly on temperature and hence the lidar can be used to infer atmospheric temperature profiles (Cooney 1972a; Melfi 1972; Vaughan et al. 1993). Raman lidars are used extensively to provide high-resolution water vapor and temperature data during measurement campaigns (e.g., Wulfmeyer and Bösenberg 1998; Leblanc and McDermid 2008; Wulfmeyer et al. 2011; Adam et al. 2016; Macke et al. 2017). Until recently, only a few Raman lidars around the world have been automated and are operated in a continuous manner for the purpose of climate monitoring or numerical weather prediction. Examples are the turn-key lidar of the Atmospheric Radiation Measurement (ARM) program at the Southern Great Plains site (Goldsmith et al. 1998), the Raman lidar for Atmospheric Moisture Sensing (RAMSES) of the German Weather Service (DWD) at the Lindenberg Observatory (Reichardt et al. 2012), and the Raman Lidar for Meteorological Observations (RALMO) operated by MeteoSwiss (Dinoev et al. 2013). We consider RALMO representative of state-of-the-art automated Raman lidars and a more detailed description is provided in the following section. Advances in laser technology have paved the way for commercial instruments, which are nowadays available (Lange et al. 2019; Fréville et al. 2015). Though operational deployment of such commercial instruments is still very rare.

The RALMO. In this section, we describe in more detail the RALMO, which was developed by the Federal Institute of Technology of Lausanne, Switzerland, in the framework of a research project (Dinoev et al. 2013). A schematic picture of the RALMO with its main elements is presented in Fig. 1. Since 2006, RALMO is operated by MeteoSwiss. As one of very few such instruments, RALMO is fully automated and operated continuously delivering a long-term average data availability of 50%. Thanks to its special design for day and nighttime operation, profiles reach typically altitudes up to 5 km AGL during the day and 12 km AGL during the night with an integration time of 30 min and a vertical resolution on the order of 100 m. Since the raw data are integrated continuously over 30 min the resulting water vapor and temperature profiles are true 30 min averages and not instantaneous values. But this is still below the breakthrough requirement for high-resolution NWP, which is 60 min. In clear-sky conditions the range is limited by the signal-to-noise ratio, which is significantly lower under the presence of the daylight. Optically thick clouds like low- and

midlevel liquid water and mixed clouds fully absorb the laser's light and hence the cloud ceiling defines the range in cloudy conditions. Despite the varying range, Raman lidars are suited to be operated continuously and retrieved water vapor and temperature profiles

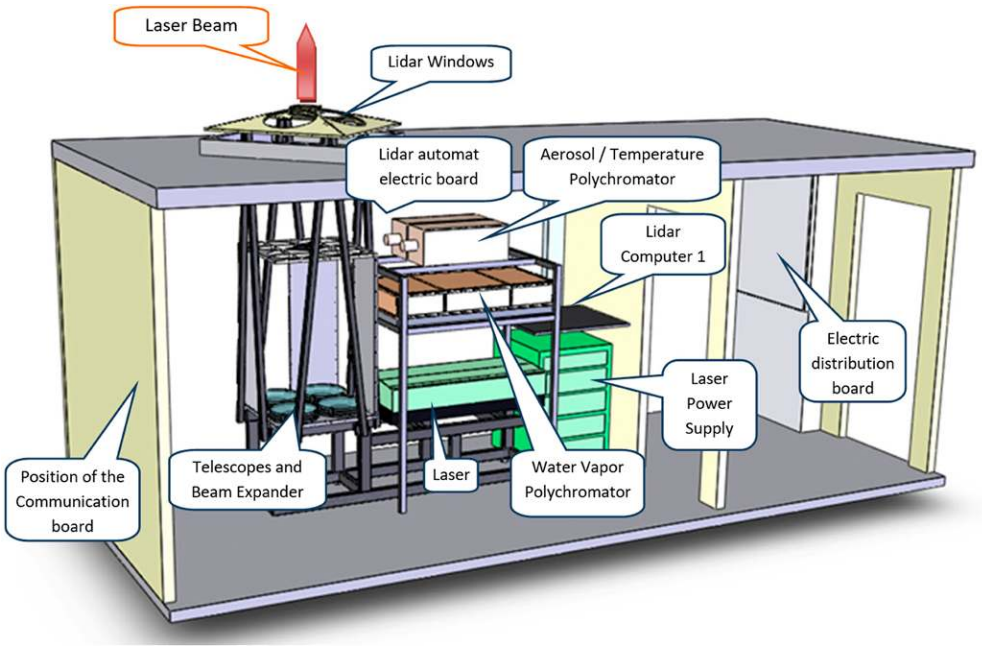

Fig. 1. Schematic picture of the Raman lidar for Meteorological Observations (RALMO) with its main elements (adapted from Dinoev et al. 2013).

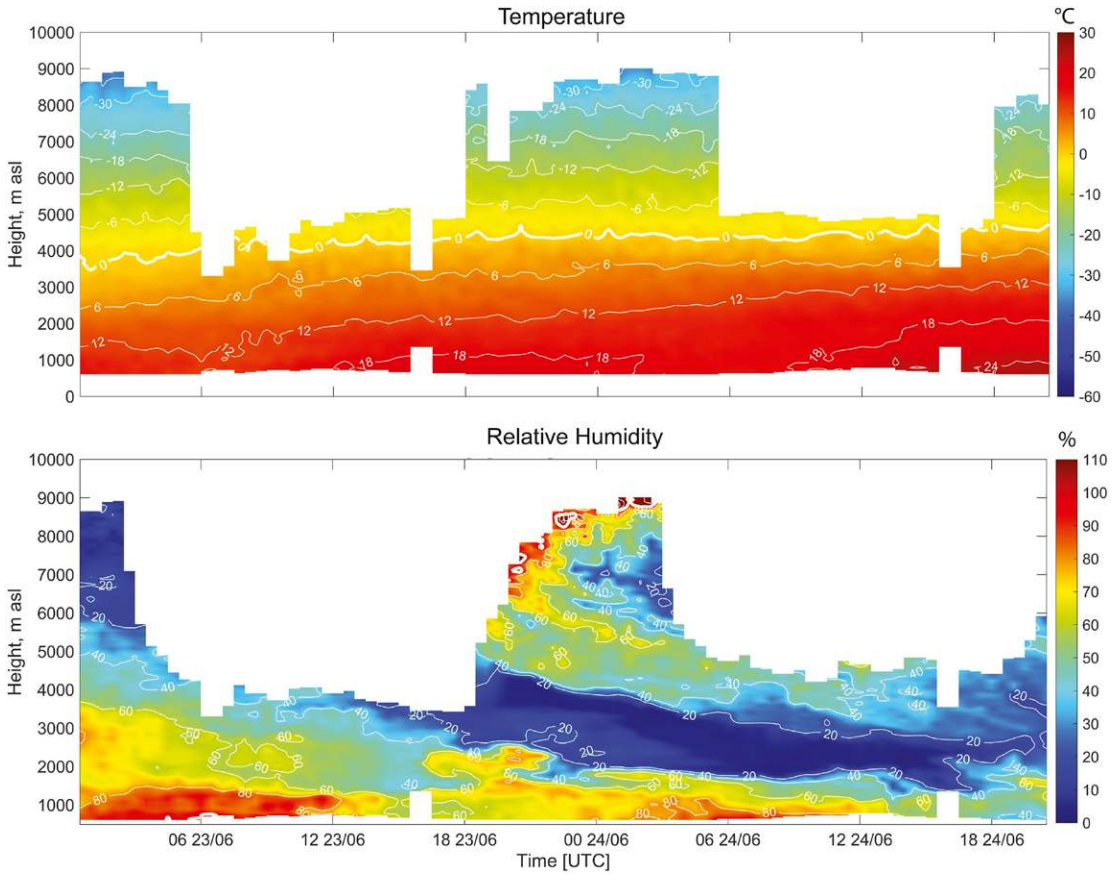

Fig. 2. Example of a Raman lidar observation time series: (top) temperature and (bottom) relative humidity evolution at Payerne, Switzerland, during two convective days on 23 and 24 Jun 2019 with a dry layer right above the boundary layer top and a humid layer above it.

can be made available in near–real time. A measurement example of relative humidity and temperature is shown in Fig. 2.

RALMO uncertainty and potential for data assimilation. The relative humidity and temperature products of RALMO have been extensively validated against radiosondes revealing a slight dry bias of 2%–4% relative humidity and essentially no bias in terms of temperature and standard deviations of 5% relative humidity and 0.5 K below 5 km, respectively (Brocard et al. 2013; Navas-Guzmán et al. 2019). Comprehensive uncertainty budgets on a profile per profile basis for water vapor mixing ratio and temperature have been established by Sica and Haefele (2016) and Mahagammulla Gamage et al. (2019). For both temperature and water vapor mixing ratio, the most important source of uncertainty is the measurement noise followed by the external calibration against a reference radiosonde.

To illustrate the potential for data assimilation into an NWP model, we established observation minus forecast ($O - F$) statistics for different initialization times and lead times. The model data has been taken from the operational deterministic analysis–forecast cycle and the statistics have been obtained from a period of 31 days starting on 1 July 2019. Figure 3 shows ($O - F$) statistics in terms of normalized interquartile range (IQR) for specific humidity for the model forecast initialized at 0000 and 2100 UTC. The interquartile range has been normalized to the average modeled specific humidity. The IQR at +0 h below 3 km is around 10% for the 0000 UTC forecast and between 15% and 30% for the 2100 UTC forecast. This large difference is explained by the fact that a radiosonde is assimilated in the 0000 UTC forecast. Further, the 0000 UTC forecast clearly reveals the growth of the model error with increasing lead time. No error growth can be found for forecasts other than 0000 and 1200 UTC, which is due to the fact that humidity information is only available at these times, the radiosondes launched at 0000 and 1200 UTC are the only data source for humidity in the lower troposphere.

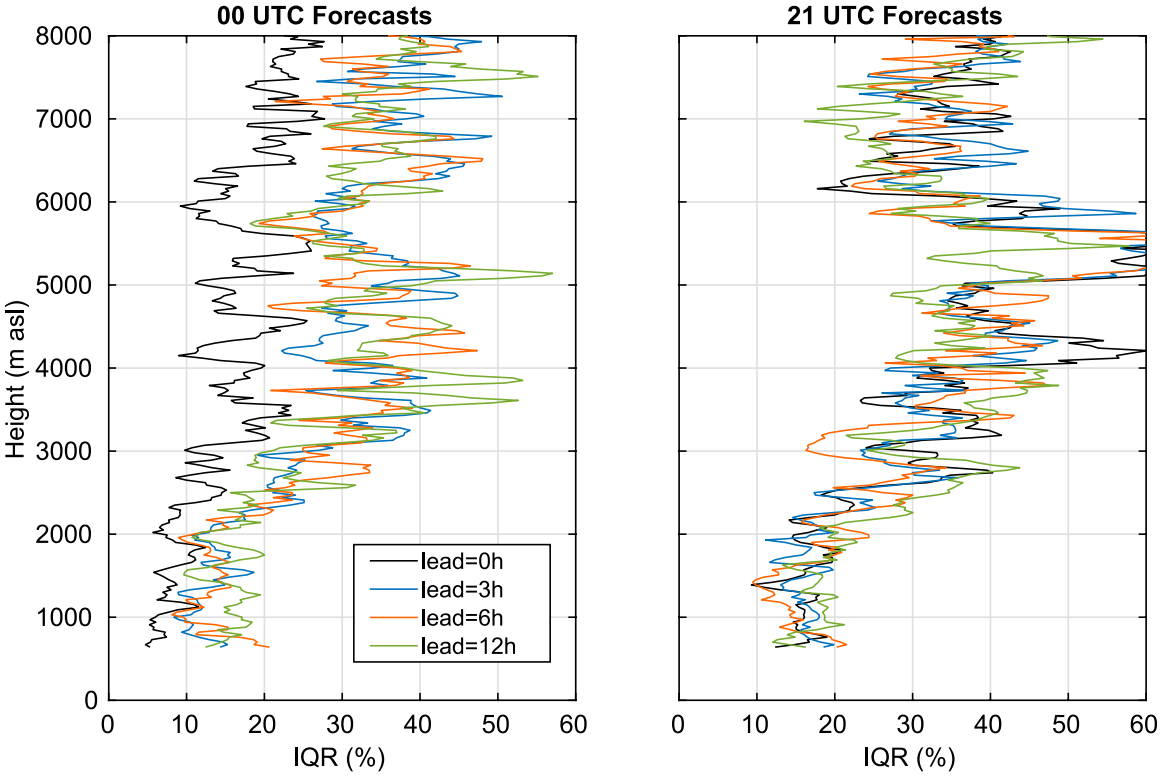

Fig. 3. Normalized interquartile range of observation minus model differences for specific humidity for forecasts initialized at (left) 0000 UTC and at (right) 2100 UTC and for lead times 0 (analysis), 3, 6, and 12 h. The interquartile range has been normalized to the average modeled specific humidity and the statistics were obtained from a period of 31 days starting on 1 Jul 2019.

Contribution to PBL observations. A deployment of a sufficiently dense operational network of Raman lidars has the potential to fill the observational gap in the lower troposphere providing temperature and humidity profiles with high vertical and temporal resolution (performance goal is 10 m and 1 min) during day and night up to at least 5 km. The RALMO observations do not only meet the threshold, but also the breakthrough requirements for high-resolution NWP according to WMO (2017) in terms of quality and vertical and temporal resolution. While lidar's emitted laser cannot penetrate clouds or fog more than few tens of meters, their measurements are particularly useful to better define the clear-sky preconvective and prefog conditions.

Drones

Short history of unmanned aerial vehicles in meteorology. In the early 1970s, Konrad et al. (1970) pioneered the use of UAVs in meteorology. The purpose of the aircraft was to gain a better understanding of convective processes. Technical progress over the years made possible the use of UAVs in different fields of atmospheric research (e.g., Holland et al. 2001; Martin et al. 2011; Mayer et al. 2012; Elston et al. 2015; Reineman et al. 2016). Martin et al. (2011), for example, used a fixed-wing UAV to fly up to 1,600 m above ground level (AGL) measuring meteorological parameters in order to investigate turbulent fluxes in the atmosphere. Reineman et al. (2016) launched UAVs from a ship to measure ocean surface processes and assimilated the observations into regional coupled ocean–atmosphere models in real time. They noted clear advantages of UAVs: sampling across atmospheric gradients, near-continuous sampling, and no limitation to airspace directly above ships. In another study by Mayer et al. (2012) the examined UAV proved e helpful insights regarding the diurnal evolution of the PBL and the identification of mesoscale features above the PBL. Moreover, the system helped to evaluate finescale atmospheric models. In a recent study, Chilson et al. (2019) outlined some of the fundamental science questions and sampling needs driving the development of an UAV network.

Meteodrones. Rotary-wing UAVs of the company Meteomatics, called Meteodrones, are hexacopters with a span of 0.6 m and measure vertical profiles of a number of meteorological quantities of the lower atmosphere at fixed locations at high temporal frequency (Fig. 4). They are easy to deploy and in contrast to radiosondes they are reusable. Flights are carried out autonomously from the Meteobase (Fig. 5): the Meteodrone is located inside the container, is released, carries out the flight and lands back on the base for recharging. This process does not require the presence of a pilot, but can be monitored by an operator from a remote operation center. In critical situations the operator can intervene and manually land a Meteodrone.

Fig. 4. Close-up of a Meteodrone. Equipped with an emergency rescue system it is allowed to fly under BVLOS (beyond visual line of sight) conditions up to 3 km AGL.

In this way, up to 10 UAVs can be supervised at the same time. A Meteodrone can gather up to four profiles per hour.

Figure 6 shows an example of Meteodrone observations during the night from 30 to 31 October 2017. The chart depicts the evolution of temperature, relative humidity, and wind speed and direction. The 20 trajectories of the UAV are indicated by the white dotted lines on the time–height chart. The evolution of the atmospheric quantities between the trajectories is not measured, but have been interpolated in time for the graphical visualization on the plot.

Flying through the lower atmosphere inevitably interferes with aviation traffic. Currently, Meteodrones operated in Switzerland are authorized by the Swiss Federal Office of Civil Aviation (FOCA) to fly up to 3 km AGL beyond visual line of sight (BVLOS) meaning the UAVs are flown beyond the visual range of the operator enabling them to cover far greater distances, vertically or horizontally. By the end of 2019 a new system will be able to fly up to 6 km AGL. The Meteodrones operationally fly up to 3 km AGL during night and up to 1.5 km during day and are allowed to enter and penetrate, but not to exit the top of the lowest cloud layer. Additionally, for every flight, a notice to airmen (NOTAM) has to be issued. The specific laws and regulations may vary significantly for other countries.

Fig. 5. Meteobase: The recently developed, fully automated launch and recharge system for the Meteodrones. The UAVs fly straight up, take their measurements, and land on the base for recharging via a connector.

Even though the Meteodrone systems are very robust, their operation can be impeded by icing conditions or high wind speeds. Icing poses a risk for UAVs as the accumulation of ice on the propellers can cause loss of control of the system. That is why tests on the effect of icing in different environments were conducted: outdoors, in an indoor ski slope and in the Vienna Climatic Wind Tunnel (Meteomatics 2017). When entering icing conditions an increase of power consumption is notable. As a solution a heating system for the propellers has been developed for the successor of the current Meteodrone. Upon onset of heating, a warming of the UAV's environment will occur. Thus, the positioning of the sensors has to take this effect into consideration. The Meteodrone sustains gusts up to 60 km h^{-1}. If it enters a region with higher wind speeds, the remote operator will be alarmed for manual intervention.

For emergency situations, every Meteodrone is equipped with an emergency rescue system (ERS) consisting of a parachute enabling a slowed-down landing. It can be manually or automatically activated for a safe landing of the UAV and to prevent it from crashing and causing damage to the surroundings and itself. A safe landing makes possible a reuse and if necessary a repair of the UAV.

Uncertainty of Meteodrones observations. In the field campaign Environmental Profiling and Initiation of Convection (EPIC) conducted by NOAA the Meteodrones observations were compared in detail to those of other UAV systems and observing systems (Koch et al. 2018). The following differences with respect to other measurements were established: a warm temperature bias of +0.4°C, dry bias of –7% RH, positive wind bias of +0.2 m s^{-1}, and a clockwise wind direction bias of 7°. The accuracy of the Meteodrone sensors mostly meet the expectations of NOAA proving the Meteodrone to be an adequate atmospheric measurement device (cf. Table 2).

However, the effect of wind speed and icing on measurement errors was not examined. Icing affects primarily the thrust, which is compensated by the UAV leading to a higher power consumption. Thus, there is no influence expected on the derivation of wind speed and direction. The response time of the different sensors ranges from 250 ms (pressure sensor) up to 4 s (relative humidity sensor). The temperature sensor has a response time below 1 s. This is sufficiently long to justify a correction algorithm to remove hysteresis effects in the ascent and descent profiles of temperature and humidity (Fengler 2017). The method requires a constant ascent and descent velocity in order to be applied.

Contribution to PBL observation. Meteodrones measure temperature, humidity, wind speed and direction, and pressure at a frequency of 4 Hz. Within 20 min of flight duration a full vertical profile of up to 3 km AGL can be observed. Typical ascent and descent rates are 3 m s^{-1}. Meteodrones are equipped with temperature and humidity sensors, comparable to those used on radiosondes. For pressure, temperature, and dewpoint temperature, an accuracy of 0.1 hPa and 0.2°C, respectively, is achieved. The wind speed and direction are derived from the aircraft's attitude data. The attitude of an UAV is determined from the inertial measurement unit data, such as the pitch and roll angle and the power needed to stabilize the UAV at a given position.

Like the lidar observations, the Meteodrone observations do not only meet the minimum but the breakthrough requirements for high-resolution NWP in terms of quality and temporal and vertical resolution according to WMO (2017).

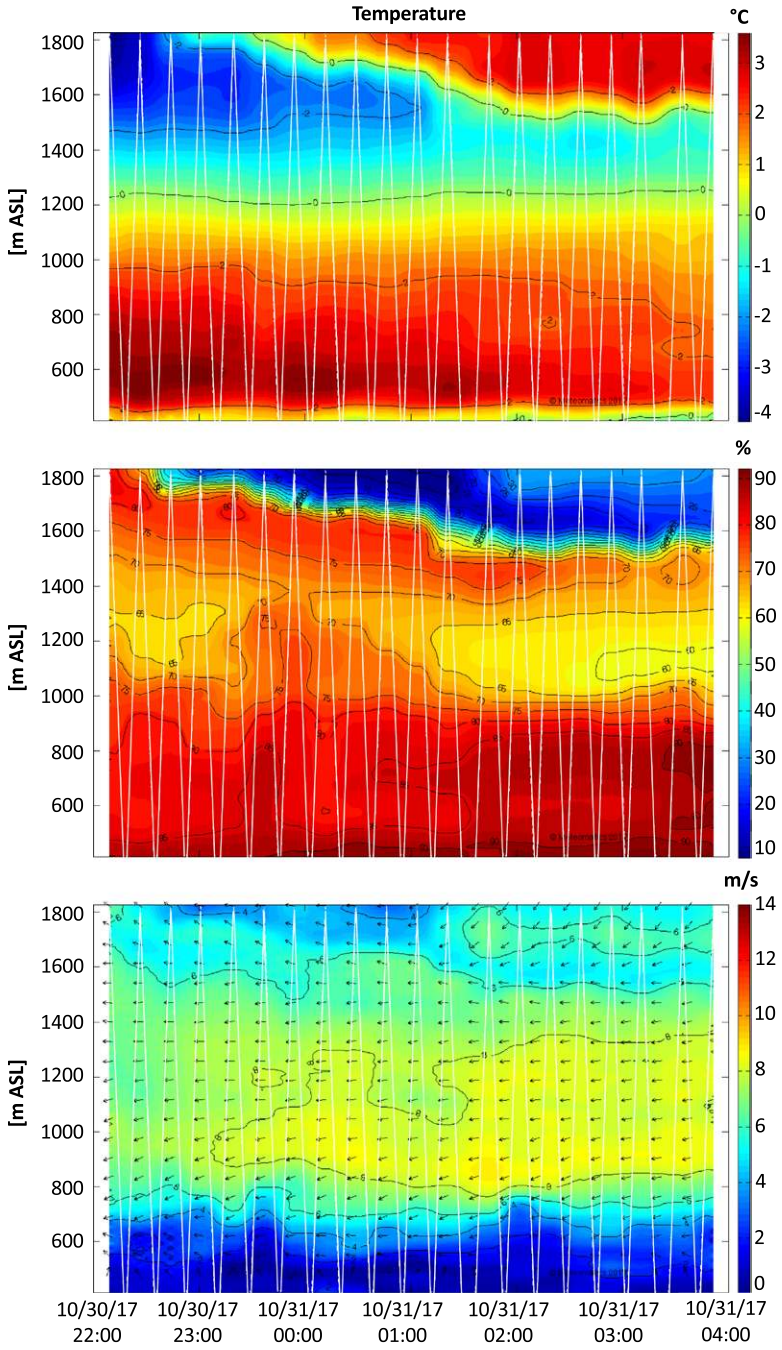

Fig. 6. Example of a Meteodrone observation time series: (top) temperature, (middle) relative humidity, and (bottom) wind speed and direction evolution in Amlikon, Switzerland, during the night of 30–31 Oct 2017. A temperature inversion at 1,200–1,800 m ASL, high relative humidity, and weak winds favored fog development in the PBL.

Impact on convective-scale numerical weather prediction

To investigate the impact of the novel observation systems to NWP analyses and forecasts, a series of

Table 2. NOAA's criteria for measurement accuracy (Koch et al. 2018).

Variable	Measurement accuracy
Temperature	±0.2°C
Relative humidity	±5.0%
Wind speed	±0.5 m s^{-1}
Wind direction	±5° azimuth
Sensor response time	<5 s (preferably <1 s)

assimilation experiments have been conducted using the operational ensemble data assimilation and NWP system of MeteoSwiss.

Thunderstorms. In the afternoon of 8 July 2017, an organized convective system associated with a cold front crossed Switzerland from west to east, causing local precipitation sums up to 80 mm over the entire weather event. A total of 24 hourly analysis cycles with and without the assimilation of RALMO profiles located at Payerne followed by a 24-h forecast were calculated. The air mass measured by the lidar and adjusted by the assimilation process in the model was advected with the southwesterly flow to regions east of the measurement location. Figure 7 shows probabilities of 24 h precipitation sums exceeding 1 mm, which is basically an information on the occurrence of precipitation. The forecast initialized with the analysis with RALMO observations shows larger probabilities of rain in the eastern part of Switzerland than that initialized from an analysis without RALMO data. Given, that rain really occurred in this region (as indicated with stippled shading in Fig. 7), the precipitation forecast clearly benefited from the additional RALMO observations in this case. Brier scores (BS) for precipitation thresholds of 1, 2, 5, 10, 20, and 50 mm 24 h^{-1} have been calculated for both forecasts on the domain depicted in Fig. 7. The forecast with lidar observations resulted in a 11.1% decrease of the BS for the 1 mm 24 h^{-1} threshold and a 6.1% decrease of the ranked probability score, which is a weighted sum of the BS for all thresholds. Another case study (convective case on 24 August 2017) exhibited a similar improvement in precipitation forecast (not shown).

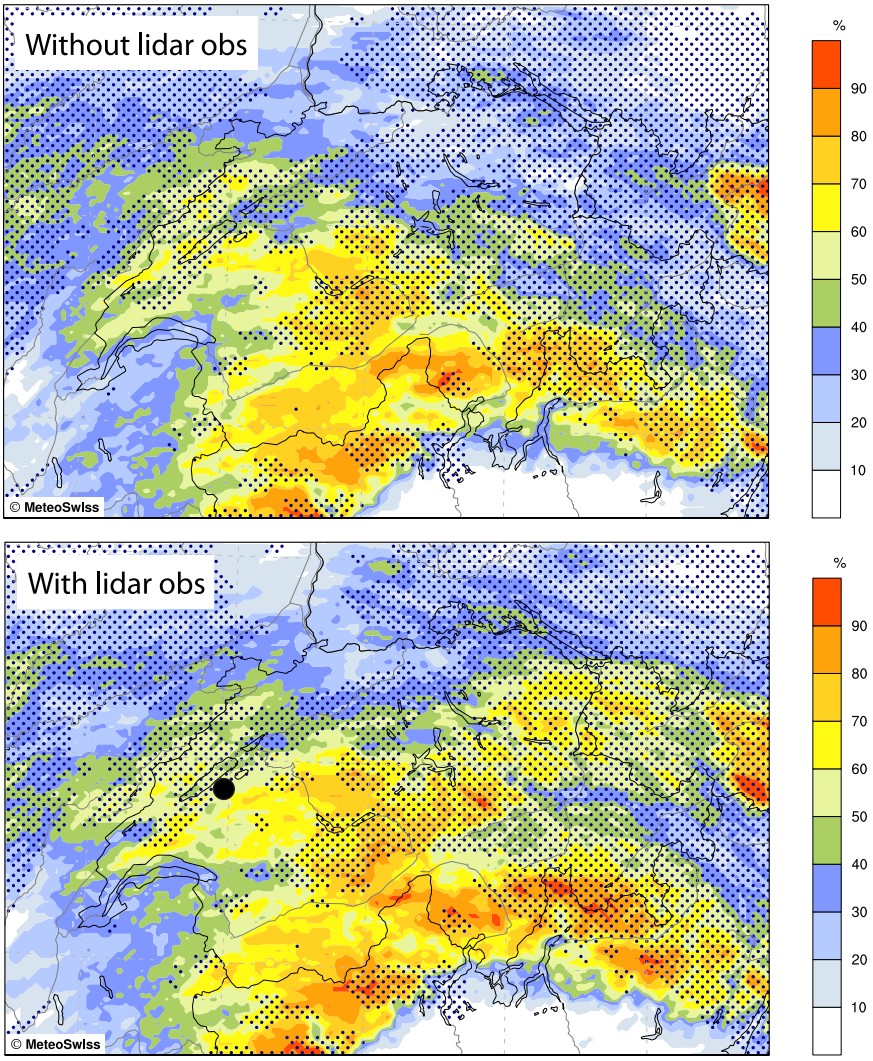

Fig. 7. Forecasted probability of the 24-h accumulated precipitation ending at 0000 UTC 9 Jul 2017 to exceed 1 mm 24 h^{-1} (color shading). Stippled shading denotes regions where the observed precipitation exceeds 1 mm 24 h^{-1}. Top (bottom) panel shows the forecast without (with) lidar observations included. A good forecast is characterized by a high probability in the stippled areas. The measurement location of Payerne is marked with a black dot in the lower panel. The forecast with lidar measurements assimilated has a better agreement of high probabilities and observed precipitation, than the one without lidar data.

Fog. During a measurement campaign in winter 2017/18, a large number of boundary layer observations have been gathered by several Meteodrones at six locations in a region of about 60 × 60 km^2 in northeastern Switzerland. From 2200 UTC in the evening to 0400 UTC in the early morning, the measurement sites were not affected by air traffic and thus could be used for probing the atmosphere up to heights of 1,800 m

AGL. At that time the Meteodrones were not yet operated automatically from the Meteobase, but required a human pilot on site. The nightly observations are ideal to target improvements of the representation of fog in the analysis, since fog often builds up during night. To assess the impact of the Meteodrones observations to NWP analyses and forecasts, seven case studies have been chosen from this measurement campaign, all correspond to situations of fog. A case with a particularly beneficial impact is described in some detail below.

On 7 December 2017 the weather in Switzerland was characterized by a high pressure system with weak synoptic-scale forcing. In such situations, the Swiss Plateau is often completely covered with fog, a typical example is shown in Fig. 8, bottom panels. With the standard set of observations, the model analysis mean substantially underestimated the fog extent (Fig. 8, top-left panel). The assimilation of the additional Meteodrones profiles located at the three positions indicated with yellow dots in Fig. 8 (middle panels) cooled and moistened the PBL and allowed the formation of fog in a region that closely resembles that of the verifying satellite image (Fig. 8, middle-left panel). Two hourly assimilation cycles from 2200 to 0000 UTC were enough to adapt the PBL in a large region. Forecasts initialized at 0000 UTC from the analyses with and without Meteodrone observations showed that the positive impact of the additional observations on the cloud forecasts lasted at least 6 h in this case (Fig. 8, right panels).

The impact of the Meteodrones observations on fog forecasts in the other six cases on 6 December 2017 and 14, 15, 16, 27, and 28 February 2018 depended on the synoptic-scale forcing of the event. In two other weak forcing events (6 December 2017 and 28 February 2018), the impact on cloudiness was clearly positive, while in three cases with a stronger synoptic-scale forcing,

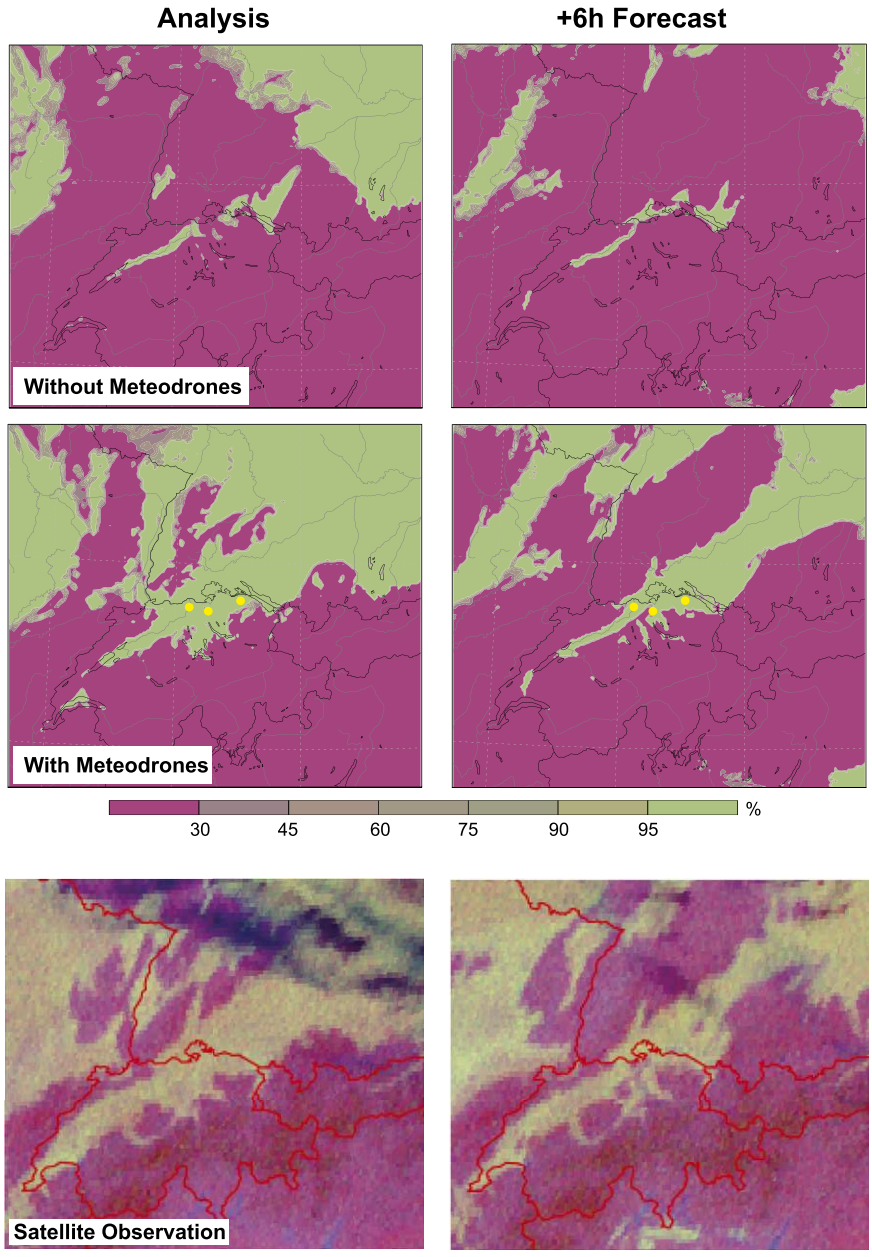

Fig. 8. Cloudiness at (left) 0000 UTC and (right) 0600 UTC 7 Dec 2017 from the COSMO ensemble mean (top) without and (middle) with the assimilation of Meteodrone observations. (left) Analysis time, and (right) +6-h forecast time. (bottom) Corresponding cloudiness as observed by satellite. Bright colors denote cloudy, purple colors cloud-free regions. The measurement locations of the Meteodrones are marked with yellow dots on the middle panels. The forecasts with Meteodrone observations assimilated shows a clearly improved cloud distribution at both, analysis and +6-h forecast time, compared to that without Meteodrone observations.

the impact was neutral. In one case, the Meteodrone observations successfully reduced an overestimated model cloud amount at the right places, suggesting that they have discriminating power for both fog enhancement and reduction. No negative impact has been found in the seven investigated cases.

Potential for a global observing system

In this section, a discussion is provided on prospects and challenges to organize Raman lidar and drones in networks for an application in regional and global NWP. Several upper-air networks have been established on a permanent basis to provide critical parameters in the PBL and lower troposphere in a continuous way for NWP applications, such as, for example, the networks in Switzerland (Calpini et al. 2011) using radar wind profilers and microwave radiometers, Japan (Kato et al. 2017) using microwave radiometers, Doppler lidars, and weather radars, and the United States (Yang and Min 2018) using Doppler lidars and microwave radiometers. Raman lidars and drones are not used in these networks, mainly because their maturity in terms of automation and reliability was not sufficient up to now. Further, a high level of expert knowledge was required to operate the systems and process and use the data correctly.

For lidars, the arrival of diode pumped lasers for Raman applications (Lange et al. 2019) and frequency stabilized diode lasers for elastic applications (Spuler et al. 2015) are about to bring automated systems to a maturity level that makes them fit for network applications. We expect acquisition costs of a Raman lidar device to be on the order of $100,000 to $500,000 (U.S. dollars) depending on system performance and annual operating costs on the order of $10,000 to $50,000.

UAVs are still a very young technology and flight regulations differ from country to country, so far hindering the establishment of a broad network. An important step toward harmonization of regulations in Europe was made by the European Union Aviation Safety Agency (EASA) with the aim of a common ground across Europe. Besides, the UAV community is on a steep learning curve concerning the technology and the variety of applications (e.g., Chilson et al. 2019). Another challenge for an UAV network is the ability for an automatic operation. The Meteobase described above is an important step toward an operational application of UAV in meteorology. The estimated costs for the automated systems are on the order of $100,000 per Meteobase and year, including hardware and operation costs.

The design of a future network of lidars and drones depends on a variety of factors, such as population density, topographic complexity, already existing other observations, and NWP configuration. The OSCAR requirement database contains not only requirements on vertical and temporal resolution of an observing system, but also on the horizontal spacing of the devices in a network. With respect to high-resolution NWP, the threshold (breakthrough) spatial-resolution requirements for temperature, humidity, and wind are 10 km (2 km) and with respect to global NWP, 500 km (100 km) for wind and temperature, and 250 km (50 km) for humidity. It is very likely that these thresholds present an upper bound of the requirements over complex topography in countries such as Switzerland. The spatial network density of a future observation system for an application in NWP is commonly estimated using observing system simulation experiments (OSSEs). An example for a UAV mesonetwork has recently been published by Chilson et al. (2019). They assimilated PBL profiles of a hypothetical network of 110 UAVs with a spacing of about 35 km. They found, that a maximum height of 1 km AGL and a reduced station set of 25 stations was sufficient to improve the analyses and forecasts of convection initiation, though the best results were achieved when using all 110 stations and profiles up to a height of 3 km AGL. These results suggest that even a network with a station spacing well above the OSCAR threshold requirement on horizontal resolution can bring a benefit for NWP. A positive impact

can be expected already with much larger distances between stations because the impact of continuous measurements spreads continuously in space. The much higher temporal resolution of the lidar and/or drone observations will certainly be beneficial compared to sporadic radiosoundings. Our assimilation results with 3 drones and only one single lidar station corroborate this.

Meteodrones are designed to measure vertical profiles at a single location. They could, dependent on the weather situation and application, also fly horizontal tracks. Koch et al. (2018) used fixed-wing UAV for this purpose. This would allow to increase the horizontal spacing of the network with the trade-off in vertical resolution. The total track length is limited by the battery capacity and the drone weight as well as air space regulations. More research is needed to find optimal measurement strategies and network densities for lidar and Meteodrone observations.

Given the technological and administrative developments described above, we believe that lidar and drones will become standard equipment for temperature and humidity profiling over the coming decade. While lidar and drones are likely to be used first to enhance observations in sensitive areas for high-resolution NWP and nowcasting applications, they might be more widely used and become an important component of the WMO Integrated Global Observing System.

Summary and concluding remarks

There is a clear gap in the current observing system for the planetary boundary layer (PBL), particularly for temperature, humidity, and wind. These quantities typically have a high spatial and temporal variability.

Raman lidar devices and rotary-wing unmanned aerial vehicles (UAVs; also referred to as drones) are novel observation systems able to fill this gap. Both observation systems provide subhourly temperature and humidity profile measurements with a vertical resolution that allows to capture sharp gradients in the PBL and meet the requirements of WMO (2017) in terms of vertical resolution, temporal frequency, and accuracy. In addition, drones provide wind profiles with the same properties and can also provide data in the horizontal direction.

Both observation systems have a data availability sufficient for operational use. The Raman lidar operated by MeteoSwiss has a long-term average data availability of 50%, which is mainly determined by the occurrence of rain and low clouds. Meteodrones observational availability is often determined by air traffic regulations, high horizontal winds, and icing on the UAV propellers.

High-impact weather, such as thunderstorms and fog are highly affected by PBL processes: low-level temperature and humidity distributions determine the convective available potential energy and the convective inhibition of the preconvective environment and determine the occurrence or absence of fog. Numerical weather prediction (NWP) models are very sensitive to PBL temperature and humidity distributions in those meteorological situations and need an accurate 4D representation of the thermodynamical fields in order to capture convection and fog in the analyses and forecasts.

A number of assimilation experiments with an operational, convective-scale NWP system have demonstrated the value of the additional PBL observations in cases of thunderstorms and fog. Only two hourly assimilation cycles and 6 profile locations in a 60×60 km^2 large region were enough to considerably improve the representation of fog in the analyses and forecasts. Improvements in cloudiness and precipitation were found to last at minimum 6 h into forecast time in the cases under consideration.

Based on the findings of the cases considered in this study, it can be expected that a continuous assimilation of lidar and drones observations into a high-resolution NWP model

will result in a more realistic PBL structure of temperature and humidity, particularly in the vicinity of the measurement station, but also in a region around it. The size of this region was up to 400 km wide in the investigated cases in our high-resolution limited area model, but can differ depending on the weather situation, in particular on the prevailing wind field.

Both lidars and drones would optimally be deployed in dense operational networks in order to fulfill the WMO thresholds for horizontal resolution. However, given the sparse current observation network, even single additional stations can improve regional, high-resolution NWP. While cost will be the main limiting factor determining the density of a future network, other considerations such as air traffic regulations may also apply. In Switzerland, a supervised, nighttime, continuously measuring drone system is already in place at one location and a fully automated drone network is currently being developed. As of today, Raman lidars are still rather rare instruments, but the rugged and easy-to-use instruments that have recently become commercially available, have the potential to rapidly change this.

Acknowledgments. All numerical experiments have been calculated at the Swiss National Supercomputing Center (CSCS). The authors appreciate the support by Christoph Schraff (DWD) in extending the KENDA system by the new observations. Many thanks to Stephanie Westerhuis and three anonymous referees for their valuable comments on an earlier version of this paper.

References

Adam, S., A. Behrendt, T. Schwitalla, E. Hammann, and V. Wulfmeyer, 2016: First assimilation of temperature lidar data into an NWP model: Impact on the simulation of the temperature field, inversion strength and PBL depth. *Quart. J. Roy. Meteor. Soc.*, **142**, 2882–2896, https://doi.org/10.1002/qj.2875.

Ashley, W., S. Strader, D. C. Dziubla, and A. Haberlie, 2015: Driving blind: Weather-related vision hazards and fatal motor vehicle crashes. *Bull. Amer. Meteor. Soc.*, **96**, 755–778, https://doi.org/10.1175/BAMS-D-14-00026.1.

Baldauf, M., A. Seifert, J. Förstner, D. Majewski, M. Raschendorfer, and T. Reinhardt, 2011: Operational convective-scale numerical weather prediction with the COSMO model: Description and sensitivities. *Mon. Wea. Rev.*, **139**, 3887–3905, https://doi.org/10.1175/MWR-D-10-05013.1.

Balsamo, G., and Coauthors, 2018: Satellite and in situ observations for advancing global Earth surface modelling: A review. *Remote Sens.*, **10**, 2038, https://doi.org/10.3390/rs10122038.

Brocard, E., R. Philipona, A. Haefele, G. Romanens, A. Mueller, D. Ruffieux, V. Simeonov, and B. Calpini, 2013: Raman Lidar for Meteorological Observations, RALMO—Part II: Validation of water vapor measurements. *Atmos. Meas. Tech.*, **6**, 1347–1358, https://doi.org/10.5194/amt-6-1347-2013.

Browning, K. A., and Coauthors, 2007: The Convective Storm Initiation Project. *Bull. Amer. Meteor. Soc.*, **88**, 1939–1956, https://doi.org/10.1175/BAMS-88-12-1939.

Calpini, B., and Coauthors, 2011: Ground-based remote sensing profiling and numerical weather prediction model to manage nuclear power plants meteorological surveillance in Switzerland. *Atmos. Meas. Tech.*, **4**, 1617–1625, https://doi.org/10.5194/amt-4-1617-2011.

Caumont, O., and Coauthors, 2016: Assimilation of humidity and temperature observations retrieved from ground-based microwave radiometers into a convective-scale NWP model. *Quart. J. Roy. Meteor. Soc.*, **142**, 2692–2704, https://doi.org/10.1002/qj.2860.

Chilson, P. B., and Coauthors, 2019: Moving towards a network of autonomous UAS atmospheric profiling stations for observations in the Earth's lower atmosphere: The 3D mesonet concept. *Sensors*, **19**, 2720, https://doi.org/10.3390/s19122720.

Cooney, J., 1972a: Measurement of atmospheric temperature profiles by Raman backscatter. *J. Appl. Meteor.*, **11**, 108–112, https://doi.org/10.1175/1520-0450(1972)011<0108:MOATPB>2.0.CO;2.

——, 1972b: Measurement of stratospheric water vapor. *J. Geophys. Res.*, **77**, 1078–1080, https://doi.org/10.1029/JC077i006p01078.

Crook, N. A., 1996: Sensitivity of moist convection forced by boundary layer processes to low-level thermodynamic fields. *Mon. Wea. Rev.*, **124**, 1767–1785, https://doi.org/10.1175/1520-0493(1996)124<1767:SOMCFB>2.0.CO;2.

Dabberdt, W. F., and Coauthors, 2005: Multifunctional mesoscale observing networks. *Bull. Amer. Meteor. Soc.*, **86**, 961–982, https://doi.org/10.1175/BAMS-86-7-961.

Dinoev, T., V. Simeonov, Y. Arshinov, S. Bobrovnikov, P. Ristori, B. Calpini, M. Parlange, and H. van den Bergh, 2013: Raman Lidar for Meteorological Observations, RALMO—Part I: Instrument description. *Atmos. Meas. Tech.*, **6**, 1329–1346, https://doi.org/10.5194/amt-6-1329-2013.

Elston, J., B. Argrow, M. Stachura, D. Weibel, D. Lawrence, and D. Pope, 2015: Overview of small fixed-wing unmanned aircraft for meteorological sampling. *J. Atmos. Oceanic Technol.*, **32**, 97–115, https://doi.org/10.1175/JTECH-D-13-00236.1.

EUMETNET, 2020: EUMETNET E-PROFILE. EUMETNET, accessed 4 February 2020, www.eumetnet.eu/activities/observations-programme/current-activities/e-profile/.

Everett, L., 2018: *The Future of Atmospheric Boundary Layer Observing, Understanding, and Modeling.* National Academies Press, 58 pp., https://doi.org/10.17226/25138.

Fengler, M., 2017: Method and device for determining physical quantities at a plurality of locations. U.S. Patent 9 696 458 B2, 9 pp., https://patentimages.storage.googleapis.com/07/9a/88/fb50aa18ddd708/US9696458.pdf.

Fréville, P., and Coauthors, 2015: Lidar developments at Clermont-Ferrand–France for atmospheric observation. *Sensors*, **15**, 3041–3069, https://doi.org/10.3390/s150203041.

Goldsmith, J. E. M., F. H. Blair, S. E. Bisson, and D. D. Turner, 1998: Turn-key Raman lidar for profiling atmospheric water vapor, clouds, and aerosols. *Appl. Opt.*, **37**, 4979–4990, https://doi.org/10.1364/AO.37.004979.

Gultepe, I., and Coauthors, 2009: The Fog Remote Sensing and Modeling field project. *Bull. Amer. Meteor. Soc.*, **90**, 341–360, https://doi.org/10.1175/2008BAMS2354.1.

Hardesty, R., and R. Hoff, 2012: Thermodynamic profiling technologies workshop report to the National Science Foundation and the National Weather Service. NCAR Tech. Note NCAR/TN-488+STR, 80 pp., https://doi.org/10.5065/D6SQ8XCF.

Holland, G. J., and Coauthors, 2001: The aerosonde robotic aircraft: A new paradigm for environmental observations. *Bull. Amer. Meteor. Soc.*, **82**, 889–901, https://doi.org/10.1175/1520-0477(2001)082<0889:TARAAN>2.3.CO;2.

Hunt, B. R., E. J. Kostelich, and I. Szunyogh, 2007: Efficient data assimilation for spatiotemporal chaos: A local ensemble transform Kalman filter. *Physica D*, **230**, 112–126, https://doi.org/10.1016/j.physd.2006.11.008.

Illingworth, A. J., and Coauthors, 2019: How can existing ground-based profiling instruments improve European weather forecasts? *Bull. Amer. Meteor. Soc.*, **100**, 605–619, https://doi.org/10.1175/BAMS-D-17-0231.1.

Kato, R., S. Shimizu, K. Shimose, and K. Iwanami, 2017: Very short time range forecasting using CReSS-3DVAR for a meso-γ-scale, localized, extremely heavy rainfall event: Comparison with an extrapolation-based nowcast. *J. Disaster Res.*, **12**, 967–979, https://doi.org/10.20965/jdr.2017.p0967.

KNMI, 2019: Mode-S EHS research. KNMI, accessed 24 October 2019, www.mode-s.knmi.nl.

Koch, S. E., M. Fengler, P. B. Chilson, K. L. Elmore, B. Argrow, D. L. Andra, and T. Lindley, 2018: On the use of unmanned aircraft for sampling mesoscale phenomena in the preconvective boundary layer. *J. Atmos. Oceanic Technol.*, **35**, 2265–2288, https://doi.org/10.1175/JTECH-D-18-0101.1.

Köhler, C., and Coauthors, 2017: Critical weather situations for renewable energies—Part B: Low stratus risk for solar power. *Renewable Energy*, **101**, 794–803, https://doi.org/10.1016/j.renene.2016.09.002.

Konrad, T., M. Hill, J. Rowland, and J. Meyer, 1970: A small, radio-controlled aircraft as a platform for meteorological sensors. *Appl. Phys. Lab. Tech. Dig.*, **10**, 11–19.

Lange, D., A. Behrendt, and V. Wulfmeyer, 2019: Compact operational tropospheric water vapor and temperature Raman lidar with turbulence resolution. *Geophys. Res. Lett.*, **46**, 14 844–14 853, https://doi.org/10.1029/2019GL085774.

Leblanc, T., and I. S. McDermid, 2008: Accuracy of Raman lidar water vapor calibration and its applicability to long-term measurements. *Appl. Opt.*, **47**, 5592–5603, https://doi.org/10.1364/AO.47.005592.

Macke, A., and Coauthors, 2017: The HD(CP)^2 Observational Prototype Experiment (HOPE)—An overview. *Atmos. Chem. Phys.*, **17**, 4887–4914, https://doi.org/10.5194/acp-17-4887-2017.

Mahagammulla Gamage, S., R. J. Sica, G. Martucci, and A. Haefele, 2019: Retrieval of temperature from a multiple channel pure rotational Raman backscatter lidar using an optimal estimation method. *Atmos. Meas. Tech.*, **12**, 5801–5816, https://doi.org/10.5194/amt-12-5801-2019.

Martin, S., J. Bange, and F. Beyrich, 2011: Meteorological profiling of the lower troposphere using the research UAV "M2AV Carolo." *Atmos. Meas. Tech.*, **4**, 705–716, https://doi.org/10.5194/amt-4-705-2011.

Mayer, S., A. Sandvik, M. O. Jonassen, and J. Reuder, 2012: Atmospheric profiling with the UAS SUMO: A new perspective for the evaluation of fine-scale atmospheric models. *Meteor. Atmos. Phys.*, **116**, 15–26, https://doi.org/10.1007/s00703-010-0063-2.

Melfi, S. H., 1972: Remote measurements of the atmosphere using Raman scattering. *Appl. Opt.*, **11**, 1605–1610, https://doi.org/10.1364/AO.11.001605.

Meteomatics, 2017: Project "SOPHIA"—Final report (study of propeller icing hazard in mini-UAV aviation). Meteomatics Rep., 71 pp., www.meteomatics

.com/wp-content/uploads/2019/02/SOPHIA%20Final%20Report-public.pdf.

National Research Council, 2010: *When Weather Matters: Science and Services to Meet Critical Societal Needs*. National Academies Press, 198 pp., https://doi.org/10.17226/12888.

Navas-Guzmán, F., G. Martucci, M. Collaud Coen, M. J. Granados-Muñoz, M. Hervo, M. Sicard, and A. Haefele, 2019: Characterization of aerosol hygroscopicity using Raman lidar measurements at the EARLINET station of Payerne. *Atmos. Chem. Phys.*, **19**, 11 651–11 668, https://doi.org/10.5194/acp-19-11651-2019.

Petersen, R. A., 2016: On the impact and benefits of AMDAR observations in operational forecasting—Part I: A review of the impact of automated aircraft wind and temperature reports. *Bull. Amer. Meteor. Soc.*, **97**, 585–602, https://doi.org/10.1175/BAMS-D-14-00055.1.

Reichardt, J., U. Wandinger, V. Klein, I. Mattis, B. Hilber, and R. Begbie, 2012: RAMSES: German meteorological service autonomous Raman lidar for water vapor, temperature, aerosol, and cloud measurements. *Appl. Opt.*, **51**, 8111–8131, https://doi.org/10.1364/AO.51.008111.

Reineman, B. D., L. Lenain, and W. K. Melville, 2016: The use of ship-launched fixed-wing UAVs for measuring the marine atmospheric boundary layer and ocean surface processes. *J. Atmos. Oceanic Technol.*, **33**, 2029–2052, https://doi.org/10.1175/JTECH-D-15-0019.1.

Rémy, S., and T. Bergot, 2009: Assessing the impact of observations on a local numerical fog prediction system. *Quart. J. Roy. Meteor. Soc.*, **135**, 1248–1265, https://doi.org/10.1002/qj.448.

Schraff, C., H. Reich, A. Rhodin, A. Schomburg, K. Stephan, A. Perianez, and R. Potthast, 2016: Kilometre-scale ensemble data assimilation for the COSMO model (KENDA). *Quart. J. Roy. Meteor. Soc.*, **142**, 1453–1472, https://doi.org/10.1002/qj.2748.

Sica, R. J., and A. Haefele, 2016: Retrieval of water vapor mixing ratio from a multiple channel Raman-scatter lidar using an optimal estimation method. *Appl. Opt.*, **55**, 763–777, https://doi.org/10.1364/AO.55.000763.

Spuler, S. M., K. S. Repasky, B. Morley, D. Moen, M. Hayman, and A. R. Nehrir, 2015: Field-deployable diode-laser-based differential absorption lidar (dial) for profiling water vapor. *Atmos. Meas. Tech.*, **8**, 1073–1087, https://doi.org/10.5194/amt-8-1073-2015.

Stephan, K., S. Klink, and C. Schraff, 2008: Assimilation of radar-derived rain rates into the convective-scale model COSMO-DE at DWD. *Quart. J. Roy. Meteor. Soc.*, **134**, 1315–1326, https://doi.org/10.1002/qj.269.

Tatem, A., S. Goetz, and S. Hay, 2008: Fifty years of Earth observation satellites. *Amer. Sci.*, **96**, 390–398, https://doi.org/10.1511/2008.74.390.

Vaughan, G., D. P. Wareing, S. J. Pepler, L. Thomas, and V. Mitev, 1993: Atmospheric temperature measurements made by rotational Raman scattering. *Appl. Opt.*, **32**, 2758–2764, https://doi.org/10.1364/AO.32.002758.

Weckwerth, T. M., and Coauthors, 2004: An overview of the International H_2O Project (IHOP_2002) and some preliminary highlights. *Bull. Amer. Meteor. Soc.*, **85**, 253–278, https://doi.org/10.1175/BAMS-85-2-253.

WMO, 2017: Observing Systems Capability Analysis and Review tool. WMO, www.wmo-sat.info/oscar/.

——, 2018a: Statement of guidance for global numerical weather prediction (NWP). WMO Rep., 12 pp., www.wmo.int/pages/prog/www/OSY/SOG/SoG-Global-NWP.pdf.

——, 2018b: Statement of guidance for high-resolution numerical weather prediction (NWP). WMO Rep., 10 pp., www.wmo.int/pages/prog/www/OSY/SOG/SoG-HighRes-NWP.pdf.

Wulfmeyer, V., and J. Bösenberg, 1998: Ground-based differential absorption lidar for water-vapor profiling: Assessment of accuracy, resolution, and meteorological applications. *Appl. Opt.*, **37**, 3825–3844, https://doi.org/10.1364/AO.37.003825.

——, and Coauthors, 2011: The Convective and Orographically-Induced Precipitation Study (COPS): The scientific strategy, the field phase, and research highlights. *Quart. J. Roy. Meteor. Soc.*, **137**, 3–30, https://doi.org/10.1002/qj.752.

Yang, J., and Q. Min, 2018: Retrieval of atmospheric profiles in the New York state mesonet using one-dimensional variational algorithm. *J. Geophys. Res. Atmos.*, **123**, 7563–7575, https://doi.org/10.1029/2018JD028272.

Zhang, X., H. Wang, X. Huang, F. Gao, and N. A. Jacobs, 2015: Using adjoint-based forecast sensitivity method to evaluate TAMDAR data impacts on regional forecasts. *Adv. Meteor.*, **2015**, 1–13, https://doi.org/10.1155/2015/427616.